ELSEVIER

Inorganica Chimica Acta 226 (1994) 61–68

Inorganica Chimica Acta

Infrared spectroelectrochemistry of $[Rh(TM4)_4M(CO)_5]_2^{2+}$ (TM4 = 2,5-diisocyano-2,5-dimethylhexane; M = Re, Mn): electron-transfer-promoted metal–metal bond cleavage and formation

Michael G. Hill, John P. Bullock, Timothy Wilson, Paul Bacon, Christine A. Blaine, Kent R. Mann *

Department of Chemistry, University of Minnesota, Minneapolis, MN 55455, USA

Received 21 March 1994

Abstract

Two tetranuclear complexes of the form $Rh_2(TM4)_4(M(CO)_5)_2^{2+}$ (TM4 = 2,5-diisocyano-2,5-dimethylhexane; M = Mn or Re) have been studied by electrochemical (CV) and IR spectroelectrochemical methods. In 0.1 M $TBA^+PF_6^-/CH_3CN$ (TBA^+ = tetrabutylammonium), $1e^-$ oxidation of $Rh_2(TM4)_4(Re(CO)_5)_2^{2+}$ produces a stable radical ($Rh_2(TM4)_4(Re(CO)_5)_2^{3+}$) that has been characterized by EPR and IR spectroscopy. Upon further oxidation, one Rh–Re bond is cleaved, resulting in the formation of $Rh_2(TM4)_4(Re(CO)_5)^{3+}$ and $Re(CO)_5(CH_3CN)^+$. The trimetallic fragment $Rh_2(TM4)_4(Re(CO)_5)^{3+}$ is reduced by a net $2e^-$ process to yield free $Rh_2(TM4)_4^{2+}$ and $Re(CO)_5^-$. These successive $2e^-$ oxidation/reduction reactions of $Rh_2(TM4)_4(Re(CO)_5)_2^{2+}$ ultimately yield a solution containing $Rh_2(TM4)_4^{2+}$, $Re(CO)_5(CH_3CN)^+$ and $Re(CO)_5^-$. For $Rh_2(TM4)_4(Mn(CO)_5)_2^{2+}$, oxidation occurs via a net $2e^-$ process to form the tetranuclear tetracation, $Rh_2(TM4)_4(Mn(CO)_5)_2^{4+}$. Further oxidation of this species results in Rh–Mn bond cleavage, giving $Rh_2(TM4)_4^{4+}$ and two equivalents of $Mn(CO)_5(CH_3CN)^+$. The initially formed, $1e^-$-oxidized radical, $Rh_2(TM4)_4(Mn(CO)_5)_2^{3+}$, has been observed transiently via fast-scan cyclic voltammetry. These ET-induced bond cleavage reactions are paralleled in the reduction chemistry of $Rh_2(TM4)_4(Mn(CO)_5)_2^{2+}$ and $Rh_2(TM4)_4(Re(CO)_5)_2^{2+}$. Reduction of both complexes occurs by a net $2e^-$ process, yielding free $Rh_2(TM4)_4^{2+}$ and $M(CO)_5^-$. Interestingly, upon oxidation at the coupled return for this irreversible process, the tetranuclear starting materials are regenerated in quantitative yield (i.e. no $M_2(CO)_{10}$ is produced). This chemistry stands in sharp contrast to the oxidations of $M(CO)_5^-$ anions, which produce $M_2(CO)_{10}$ in the absence of $Rh_2(TM4)_4^{2+}$. We suggest that oxidation of $Rh_2(TM4)_4^{2+}$, $M(CO)_5^-$ tight ion aggregates produce $M(CO)_5$ radicals that are entirely scavenged by $Rh_2(TM4)_4^{2+}$ to form the tetranuclear species.

Keywords: Spectroelectrochemistry; Electron transfer; Rhodium complexes; Isocyanide complexes

1. Introduction

Tetranuclear species of rhodium (e.g. $Rh_4(bridge)_8^{6+}$ (bridge = 1,3-diisocyanopropane)) [1] and platinum ('platinum blues') [2] have been discussed in terms of metal–metal bonding. Some years ago [3], we discovered a heterometallic tetranuclear species, $Rh_2(TM4)_4(M(CO)_5)_2^{2+}$ (where TM4 = 2,5-diisocyano-2,5-dimethylhexane; M = Mn or Re), formed by the 'oxidative additions' of $M_2(CO)_{10}$ dimers across the d^8–d^8 binuclear species $Rh_2(TM4)_4^{2+}$. We anticipated that redox processes in these compounds would be particularly interesting because electron transfer in and out of the frontier molecular orbitals could be coupled to changes in three metal–metal 'bonds'. IR spectroelectrochemical methods were applied to address this question, as they are ideally suited for characterizing the species generated by the electrode processes of these molecules. The frequencies of the carbonyl and isocyanide vibrational transitions are sensitive probes for estimating relative changes in the electron densities of the rhenium/manganese and rhodium atoms, respectively. By measuring the patterns and relative shifts of these stretching frequencies, we have determined the electrochemical products and have developed a qualitative picture of the metal-centered redox processes of these compounds.

* Corresponding author.

SSDI 0020-1693(94)04071-3

2. Experimental

2.1. Preparation of compounds

All solvents used for synthesis were of reagent grade quality, and were used without further purification. $Mn(CO)_{10}$ and $Re_2(CO)_{10}$ were purchased from Strem Chemicals, and sublimed prior to use. The TM4 ligand, as well as $Rh_2(TM4)_4(PF_6)_2$, $Rh_2(TM4)_2$-$Mn_2(CO)_{10}(PF_6)_2$ and $Rh_2(TM4)_4Re_2(CO)_{10}(PF_6)_2$, were prepared as previously described [3,4].

2.2. Electrochemistry

All electrochemical experiments were performed with a Bioanalytical Systems (BAS) model 100 electrochemical analyzer. Cyclic voltammetry (CV) was performed at 20 ± 2 °C with a normal three-electrode configuration consisting of a highly polished glassy-carbon-disk working electrode ($A = 0.07$ cm^2), and an AgCl/Ag reference electrode containing 1.0 M KCl. The working compartment of the electrochemical cell was separated from the reference compartment by a modified Luggin capillary. All three compartments contained a 0.1 M solution of supporting electrolyte.

Acetonitrile (Burdick and Jackson) was distilled from P_2O_5 prior to use. Tetrabutylammonium hexafluorophosphate ($TBA^+PF_6^-$) (Southwestern Analytical) was used as received. Electrolyte solutions were prepared and stored over 80–200 mesh activated alumina (Fisher Scientific Co.) and activated 4 Å molecular sieves.

Potentials are reported versus aqueous AgCl/Ag and are not corrected for the junction potential [5]. Under conditions identical to those employed here, the ferrocenium/ferrocene couple [6] has an $E^{o\prime} = +0.50$ V with $E_{pa} - E_{pc} = 94$ mV at $\nu = 100$ mV s^{-1}.

2.3. Spectroelectrochemistry

IR spectroelectrochemistry was carried out in specular reflectance mode, using a modified commercial flow-through cell [7]. The working electrode consisted of a highly polished platinum disk similar in design to that reported by Clark and co-workers [8]. Data were collected on a Mattson Galaxy 6020 FTIR spectrometer during a slow (2–8 mV s^{-1}) linear potential sweep.

X-band EPR spectra were recorded on a Bruker ESR-100 instrument.

3. Results

$Rh_2(TM4)_4(Mn(CO)_5)_2^{2+}$ and $Rh_2(TM4)_4(Re(CO)_5)_2^{2+}$ are formed by the formal oxidative additions of $M_2(CO)_{10}$ across the Rh(I)–Rh(I) complex, $Rh_2(TM4)_4^{2+}$ [3,4]. As outlined in Scheme 1, this process proceeds by photochemical bond cleavage of the d^7–d^7 metal carbonyls (via excitation into the σ–σ^* absorption), followed by addition of the $17e^-$ $M(CO)_5$ radicals to the Rh_2^{2+} core.

$$M_2(CO)_{10} \xrightarrow{h\nu} 2^{\cdot}M(CO)_5$$

$$2^{\cdot}M(CO)_5 + Rh_2(TM4)_4^{2+} \longrightarrow Rh_2(TM4)_4(M(CO)_5)_2^{2+}$$

Scheme 1. Preparation of $Rh_2(TM4)_4(M(CO)_5)_2^{2+}$ complexes.

A schematic representation of the resulting 'M(−I)–Rh(II)–Rh(II)–M(−I)' compounds is shown in Fig. 1.

The IR stretching frequencies of $Rh_2(TM4)_4$-$(Mn(CO)_5)_2^{2+}$ and $Rh_2(TM4)_4(Re(CO)_5)_2^{2+}$ are summarized in Table 1. Each compound exhibits two carbonyl stretches, and one isocyanide stretch that is characteristic of other Rh(I)–Rh(I) diisocyanide-bridged compounds [4]. The carbonyl region is typical for monosubstituted pseudo-octahedral $M(CO)_5L$ species, with the higher-energy band corresponding to one of the two A_1 stretching modes and the lower-energy

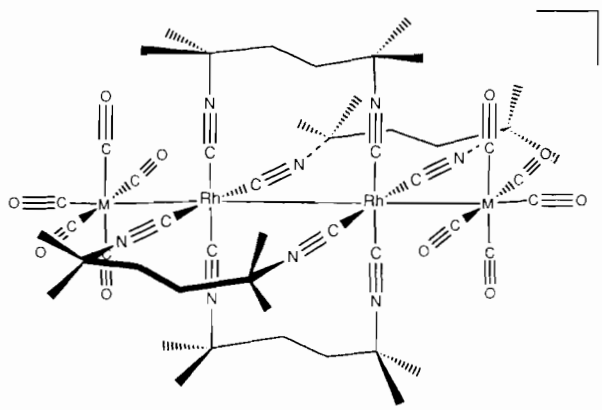

Fig. 1. Schematic representation of $Rh_2(TM4)_4(M(CO)_5)_2^{2+}$ complexes.

Table 1
IR stretching frequencies of $Rh_2(TM4)_4(M(CO)_5)_2^{2+}$ and related complexes

Complex	ν(CN) (cm^{-1})	ν(CO) (cm^{-1})
$Rh_2(TM4)_4(Re(CO)_5)_2^{2+}$	2166	2063, 1987
$Rh_2(TM4)_4(Re(CO)_5)_2^{3+}$	2181	2111, 2019, 1996(sh)
$Rh_2(TM4)_4(Re(CO)_5)^{3+}$	2189, 2160	2130
$Re_2(CO)_{10}$		2072, 2012, 1967
$Re(CO)_5(CH_3CN)^+$		2170(vw), 2062, 2035(w)
$Re(CO)_5^-$		1917, 1863
$Rh_2(TM4)_4(Mn(CO)_5)_2^{2+}$	2180	2037, 1975
$Rh_2(TM4)_4(Mn(CO)_5)_2^{4+}$	2199	2089, 2008
$Mn_2(CO)_{10}$		2047, 2012, 1981
$Mn(CO)_5(CH_3CN)^+$		2160(vw), 2074, 2052
$Mn(CO)_5^-$		1901, 1863
$Rh_2(TM4)_4^{2+}$	2160	
$Rh_2(TM4)_4(NCCH_3)_2^{4+}$	2225	

peak resulting from the overlap of the second A_1 mode and the E mode (in C_{4v} symmetry) [9]. The absence of any additional carbonyl or isocyanide stretches except those expected for isolated $M(CO)_5L$ and $M_2(L)_4$ units indicates that there is essentially no vibrational coupling between the capping groups and the central $Rh_2(TM4)_4$ unit.

On the basis of these spectra, an 'oxidative addition' description of the oxidation states of the tetranuclear species at M(−I) and Rh(II) is misleading. For example, the ν(CN) stretch of $Rh_2(TM4)_4^{2+}$ (2160 cm^{-1}) shifts only 6 and 20 cm^{-1} to higher energy upon 'oxidative addition' of $Re_2(CO)_{10}$ and $Mn_2(CO)_{10}$ across the Rh(I)–Rh(I) core (compared to a 53 cm^{-1} shift in ν(CN) upon oxidative addition of Cl_2) [10]. Moreover, the ν(CO) stretches of the $M(CO)_5$ moieties of the tetranuclears (2063 and 1989 cm^{-1} for Re; 2037 and 1975 cm^{-1} for Mn) are much higher than those for free $M(CO)_5^-$ (1917 and 1863 cm^{-1} for Re; 1901 and 1863 cm^{-1} for Mn) and, in fact, are closer in energy to the peaks of $M_2(CO)_{10}$ (2012 and 1967 cm^{-1} for Re; 2012 and 1981 cm^{-1} for Mn; Table 1). Thus a better approximation of the metal oxidation states is probably M(0)–Rh(I)–Rh(I)–M(0). These small changes in the ν(CN) and ν(CO) stretching frequencies and the rich redox chemistry exhibited by $M_2(CO)_{10}$ [11–16] and Rh_2(diisocyanide)$_4^{2+}$ [17] suggested that the tetranuclears would exhibit extensive oxidation and reduction chemistry.

Fig. 2 shows the cyclic voltammogram (CV) of $Rh_2(TM4)_4(Re(CO)_5)_2^{2+}$ in 0.1 M $TBA^+PF_6^-/CH_3CN$. This complex undergoes a quasi-reversible $1e^-$ oxidation ($E^{\circ\prime}_{3+/2+} = +0.54$ V) followed by an irreversible $1e^-$ oxidation ($E_{pa} = +0.98$ V) with a coupled return at −0.27 V. The IR spectral changes accompanying these oxidations are shown in Fig. 3. As the potential is swept through the first process, peaks due to the $Rh_2(TM4)_4(Re(CO)_5)_2^{2+}$ starting material (ν(CO) = 2063 and 1987 cm^{-1}; ν(CN) = 2166 cm^{-1}) decrease in intensity to give four new bands (ν(CO) = 1996(sh), 2019 and 2111 cm^{-1}; ν(CN) = 2181 cm^{-1}). The conversion of the dication to the radical trication is clean, as evidenced by isosbestic points at 2174, 2135, 2048 and 1999 cm^{-1}.

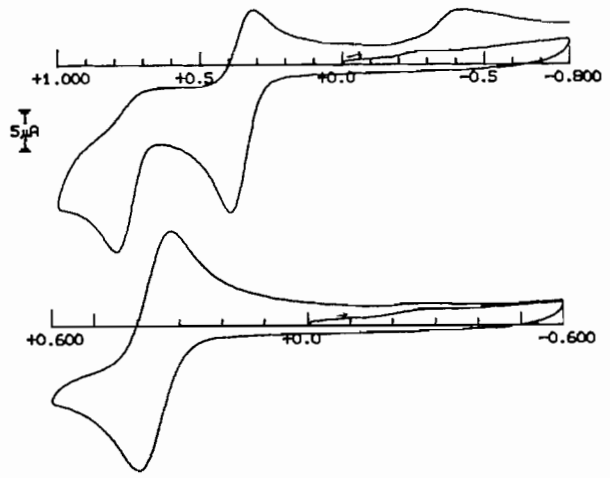

Fig. 2. Cyclic voltammograms of $Rh_2(TM4)_4(Re(CO)_5)_2^{2+}$ in 0.1 M $TBA^+PF_6^-/CH_3CN$ at a scan rate of 0.100 V s^{-1}.

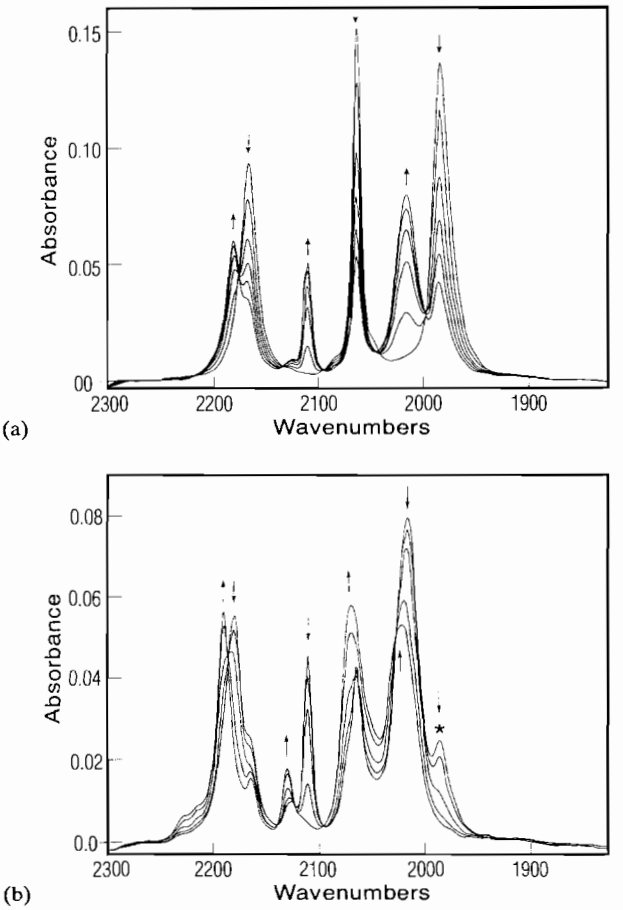

Fig. 3. IR spectroelectrochemical oxidation of $Rh_2(TM4)_4(Re(CO)_5)_2^{2+}$ in 0.1 M $TBA^+PF_6^-/CH_3CN$. (a) Spectra recorded during a slow potential sweep (8 mV s^{-1}) through the first oxidation process. (b) Spectra recorded during a slow potential sweep (8 mV s^{-1}) through the second oxidation process. The starred peak is due to some $Rh_2(TM4)_4(Re(CO)_5)_2^{2+}$ remaining from (a).

The most obvious change in the IR spectrum upon oxidation is the dramatic shift in the carbonyl stretching frequencies relative to those of the isocyanides: $\Delta\nu(CO) = \nu(CO)(Rh_2Re_2^{3+}) - \nu(CO)(Rh_2Re_2^{2+}) = 35$ (A_1 mode) and 48 cm^{-1} (E mode) versus $\Delta\nu(CN) = \nu(CN)(Rh_2Re_2^{3+}) - \nu(CN)(Rh_2Re_2^{2+}) = 15$ cm^{-1}. These data provide strong evidence that the first oxidation of $Rh_2(TM4)_4(Re(CO)_5)_2^{2+}$ occurs primarily at rhenium and produces a delocalized $Rh_2(TM4)_4(Re(CO)_5)_2^{3+}$ radical with equivalent rhenium centers. This assignment is further supported by the EPR spectrum of $Rh_2(TM4)_4(Re(CO)_5)_2^{3+}$ recorded in frozen (77 K) 0.1 M $TBA^+PF_6^-/CH_3CN$ solution (Fig. 4). A

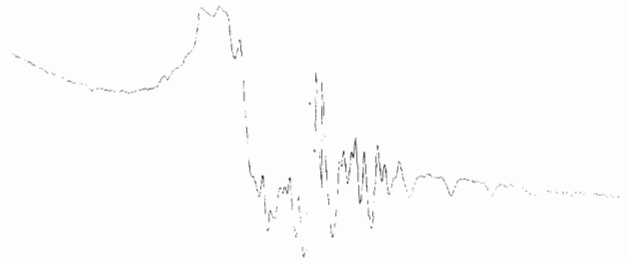

Fig. 4. EPR spectrum of $Rh_2(TM4)_4(Re(CO)_5)_2^{3+}$ in 0.1 M $TBA^+PF_6^-/CH_3CN$ frozen at 77 K. The spectrum is from 1600 to 4600 G at $\nu = 9.2766$ GHz.

preliminary analysis of this spectrum [1] clearly indicates that the unpaired electron is delocalized over two equivalent $Re(CO)_5$ fragments, with very little interaction with the Rh_2 central core.

Sweeping the potential positive of the second oxidation of $Rh_2(TM4)_4(Re)(CO)_5)_2^{2+}$ yields the spectral changes shown in Fig. 3(b). Five new peaks grow in at higher energy ($\nu(CO) = 2023$, 2062 and 2130 cm^{-1}; $\nu(CN) = 2189$ and 2164 cm^{-1}). The IR stretch at 2062 cm^{-1} is characteristic of free $Re(CO)_5(CH_3CN)^+$ [16], indicating that oxidation of $Rh_2(TM4)_4(Re(CO)_5)_2^{3+}$ is accompanied by Rh–Re bond cleavage to produce $Re(CO)_5(CH_3CN)^+$. The remaining absorbances are assigned to a trinuclear species, $Rh_2(TM4)_4Re(CO)_5^{3+}$. Based on the frequencies of these stretches, the trinuclear trication is probably best described as a highly delocalized Rh(I)–Rh(I)–Re(I) species. Interestingly, reduction of $Rh_2(TM4)_4Re(CO)_5^{3+}$ occurs by an irreversible $2e^-$ process [2] to yield $Rh_2(TM4)_4^{2+}$ and $Re(CO)_5^-$. Because the reduction of $Rh_2(TM4)_4Re(CO)_5^{3+}$ ($E_{pa} = -0.27$ V) is more positive than that of $Re(CO)_5(CH_3CN)^+$ ($E_{pa} = -1.29$ V) [16], reduction of the $2e^-$-oxidized solution back to its initial electron count completes a net electron-transfer cycle in which the tetranuclear $Rh_2(TM4)_4(Re(CO)_5)_2^{2+}$ complex is split into $Rh_2(TM4)_4^{2+}$, $Re(CO)_5(CH_3CN)^+$ and $Re(CO)_5^-$ (Scheme 2). Combining Schemes 1 and 2, the redox chemistry described above constitutes a net photo-electrochemical disproportionation of $Re_2(CO)_{10}$.

[1] Qualitatively, this spectrum can be fit to a spin-1/2 system with a rhombic g tensor ($g_1 \approx 3.5$, $g_2 \approx 3.0$, $g_3 \approx 2.3$) and ^{187}Re (spin 5/2) hyperfine splittings of $A_1 \approx 50$, $A_2 \approx 100$, and $A_3 \approx 250$ G. While we have not performed an exact simulation of this spectrum, the above parameters account for the general line shape and splitting pattern found in Fig. 4. Specifically, the large rhenium coupling constants evident in the spectrum indicate that the unpaired electron resides largely on the rhenium centers.

[2] The IR data clearly show the clean formation of $Re(CO)_5^-$ during the initial stages of the electrochemical reduction of $Rh_2(TM4)_4(Re(CO)_5)^{3+}$. However, as the concentration of $Re(CO)_5^-$ builds up in solution, peaks due to $Re_2(CO)_{10}$ (presumably formed via comproportionation of $Re(CO)_5^-$ and $Re(CO)_5(CH_3CN)^+$) and other oligomeric materials (e.g. $Re_3(CO)_{14}^{2-}$) grow in [18].

$$Rh_2(TM4)_4(Re(CO)_5)_2^{2+} \xrightarrow[E^{o\prime} = +0.54\ V]{-e^-} Rh_2(TM4)_4(Re(CO)_5)_2^{3+}$$

$$Rh_2(TM4)_4(Re(CO)_5)_2^{3+} + CH_3CN \xrightarrow[E_{pa} = +0.98\ V]{-e^-} Re(CO)_5(CH_3CN)^+ + Rh_2(TM4)_4Re(CO)_5^{3+}$$

$$Rh_2(TM4)_4Re(CO)_5^{3+} \xrightarrow[E_{pc} = -0.27\ V]{+2e^-} Re(CO)_5^- + Rh_2(TM4)_4^{2+}$$

Net:

$$Rh_2(TM4)_4(Re(CO)_5)_2^{2+} + CH_3CN \xrightarrow[(ii)\ +2e^-]{(i)\ -2e^-} Rh_2(TM4)_4^{2+} + Re(CO)_5^- + Re(CO)_5(CH_3CN)^+$$

Scheme 2. Net chemistry resulting from initial oxidation of $Rh_2(TM4)_4(Re(CO)_5)_2^{2+}$.

We have also investigated the oxidation chemistry of $Rh_2(TM4)_4(Mn(CO)_5)_2^{2+}$ in 0.1 M $TBA^+PF_6^-/CH_3CN$. At slow sweep rates ($\nu \lesssim 0.1$ V s^{-1}), this complex undergoes an irreversible oxidation ($E_{pa} = +0.47$ V), coupled to a cathodic return at -0.18 V. Bulk electrolysis at $+0.7$ V results in the passage of 1.7 e^-/tetranuclear. At faster scan rates ($\nu \gtrsim 5$ V s^{-1}), the oxidation becomes quasi-reversible, and a new irreversible process appears at $+0.98$ V, again with a coupled return at -0.18 V. We suggest that at fast scan rates, $Rh_2(TM4)_4(Mn(CO)_5)_2^{2+}$ is reversibly oxidized to $Rh_2(TM4)_4(Mn(CO)_5)_2^{3+}$; at slow scan rates, this radical species disproportionates to give a net 2 electron process. The large peak separation may be due to a large Rh–Rh bond length change that is coupled to the second electron transfer.

The IR spectral changes that occur during these processes are shown in Fig. 5. Initial bands at 2180, 2037 and 1975 cm^{-1} give way to three new bands:

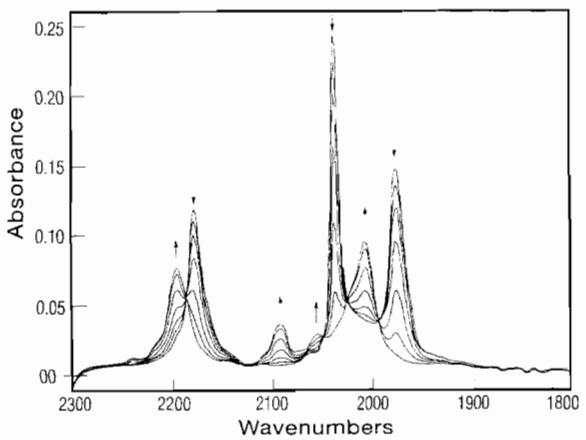

Fig. 5. IR spectroelectrochemical oxidation of $Rh_2(TM4)_4(Mn(CO)_5)_2^{2+}$ in 0.1 M $TBA^+PF_6^-/CH_3CN$. Spectra were recorded during a slow linear potential sweep through the first oxidation process of $Rh_2(TM4)_4(Mn(CO)_5)_2^{2+}$.

2090, 2008 (ν(CO)); 2195 (ν(CN) cm^{-1}). Based on the coulometry data, we assign this spectrum to the doubly oxidized tetranuclear $Rh_2(TM4)_4(Mn(CO)_5)_2^{4+}$; indeed, rapid-scan IR spectra obtained during the early stages of the spectroelectrochemical oxidation reveal a transient feature at 2189 cm^{-1}, presumably due to the initial formation of $Rh_2(TM4)_4(Mn(CO)_5)_2^{3+}$. Reduction of $Rh_2(TM4)_4(Mn(CO)_5)_2^{4+}$ at potentials negative of the coupled return at -0.18 V in the CV regenerates the $Rh_2(TM4)_4(Mn(CO)_5)_2^{2+}$ starting material in nearly quantitative yield. Further oxidation of $Rh_2(TM4)_4(Mn(CO)_5)_2^{4+}$ ($E_{app} > +1.5$ V) results in metal–metal bond cleavage, giving the d^7–d^7 complex $Rh_2(TM4)_4(NCCH_3)_2^{4+}$ (ν(CN) = 2225 cm^{-1}) and two equivalents of $Mn(CO)_5(CH_3CN)^+$ (ν(CO) = 2076 and 2056 cm^{-1}). These processes are summarized in Scheme 3.

$$Rh_2(TM4)_4(Mn(CO)_5)_2^{2+} \underset{+2e^-\,(E_{pc} = -0.18\ V)}{\overset{-2e^-\,(E_{pa} = +0.47\ V)}{\rightleftharpoons}} Rh_2(TM4)_4(Mn(CO)_5)_2^{4+}$$

$$Rh_2(TM4)_4(Mn(CO)_5)_2^{4+} + 2CH_3CN \xrightarrow[E_a > +1.5\ V]{-2e^-} Rh_2(TM4)_4(NCCH_3)_2^{4+} + 2Mn(CO)_5(CH_3CN)^+$$

Scheme 3. Net chemistry resulting from initial oxidation of $Rh_2(TM4)_4(Mn(CO)_5)_2^{2+}$.

In contrast to the differences in the oxidation chemistry of $Rh_2(TM4)_4(Mn(CO)_5)_2^{2+}$ and $Rh_2(TM4)_4(Re(CO)_5)_2^{2+}$, the electrochemical reductions of each species are similar. Both show an irreversible $2e^-$ process ($E_{pc} = -1.00$ V, $Rh_2(TM4)_4(Mn(CO)_5)_2^{2+}$; $E_{pc} = -1.25$ V, $Rh_2(TM4)_4(Re(CO)_5)_2^{2+}$), coupled to an anodic return at more positive potentials ($E_{pa} = -0.16$ V, $Rh_2(TM4)_4(Mn(CO)_5)_2^{2+}$; $E_{pa} = -0.47$ V, $Rh_2(TM4)_4(Re(CO)_5)_2^{2+}$). The reduction chemistry of $Rh_2(TM4)_4(Mn(CO)_5)_2^{2+}$ and $Rh_2(TM4)_4^{2+}$ in the presence of $Mn_2(CO)_{10}$ is summarized in Scheme 4.

$$Rh_2(TM4)_4(Mn(CO)_5)_2^{2+} \underset{-2e^-}{\overset{+2e^-}{\rightleftharpoons}} Rh_2(TM4)_4^{2+} + 2Mn(CO)_5^-$$

In the presence of $Mn_2(CO)_{10}$:

$$Mn_2(CO)_{10} \underset{-2e^-}{\overset{+2e^-}{\rightleftharpoons}} 2Mn(CO)_5^-$$

$$Mn_2(CO)_{10} + Rh_2(TM4)_4^{2+} \xrightarrow{+2e^-} 2Mn(CO)_5^- + Rh_2(TM4)_4^{2+}$$

$$2Mn(CO)_5^- + Rh_2(TM4)_4^{2+} \xrightarrow{-2e^-} Mn_2(CO)_{10} + Rh_2(TM4)_4^{2+}$$

Scheme 4. Reduction chemistry of $Rh_2(TM4)_4(Mn(CO)_5)_2^{2+}$.

Fig. 6(a) shows the IR spectroelectrochemical reduction of $Rh_2(TM4)_4(Mn(CO)_5)_2^{2+}$ in 0.1 M $TBA^+PF_6^-$/CH_3CN. As bands due to the starting material disappear,

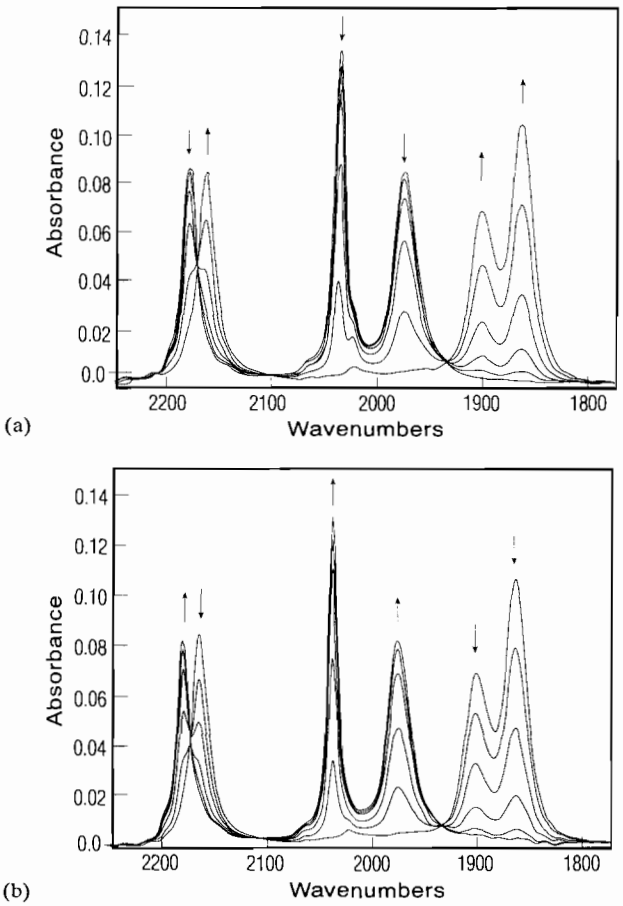

Fig. 6. (a) IR spectroelectrochemical reduction of $Rh_2(TM4)_4(Mn(CO)_5)_2^{2+}$ in 0.1 M $TBA^+PF_6^-$/CH_3CN at -1.20 V. (b) IR spectroelectrochemical oxidation of the products of (a).

three new features grow in at lower energy (ν(CN) = 2160 cm^{-1}, ν(CO) = 1863 and 1901 cm^{-1}). Based on the energies of these absorptions, we assign the 2160 cm^{-1} stretch to free $Rh_2(TM4)_4^{2+}$, and the 1901 and 1863 cm^{-1} stretches to $Mn(CO)_5^-$. Interestingly, oxidation of this solution regenerates $Rh_2(TM4)_4(Mn(CO)_5)_2^{2+}$ in quantitative yield (Fig. 6(b)). Indeed, $Rh_2(TM4)_4(Mn(CO)_5)_2^{2+}$ can be efficiently prepared by first reducing $Mn_2(CO)_{10}$, then oxidizing the resulting $Mn(CO)_5^-$ anion in the presence of $Rh_2(TM4)_4^{2+}$ (Fig. 7).

This chemistry stands in sharp contrast to the redox behavior of $Mn_2(CO)_{10}$ [11] and $Re_2(CO)_{10}$ [16] in the absence of $Rh_2(TM4)_4^{2+}$. For example, $Mn_2(CO)_{10}$ undergoes an irreversible $2e^-$ reduction at ~ -1.0 V in CH_3CN, coupled to an anodic return at ~ -0.3 V. IR spectroelectrochemistry confirms that reduction occurs by a net $2e^-$ process to yield $Mn(CO)_5^-$ (Fig. 8(a)), and that oxidation of the $Mn(CO)_5^-$ reduction product regenerates $Mn_2(CO)_{10}$ in very high yield

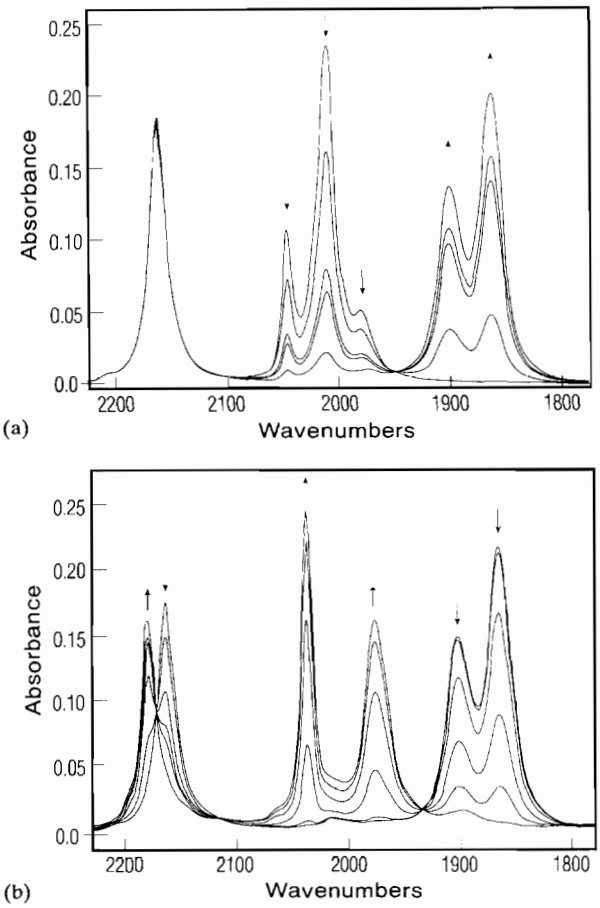

Fig. 7. (a) IR spectroelectrochemical reduction of $Mn_2(CO)_{10}$ in the presence of $Rh_2(TM4)_4^{2+}$. The product bands at 1901 and 1863 cm^{-1} are due to $Mn(CO)_5^-$. (b) IR spectroelectrochemical oxidation of the products of (a). The final spectrum with bands at 2180, 2037 and 1975 cm^{-1} is due to $Rh_2(TM4)_4(Mn(CO)_5)_2^{2+}$.

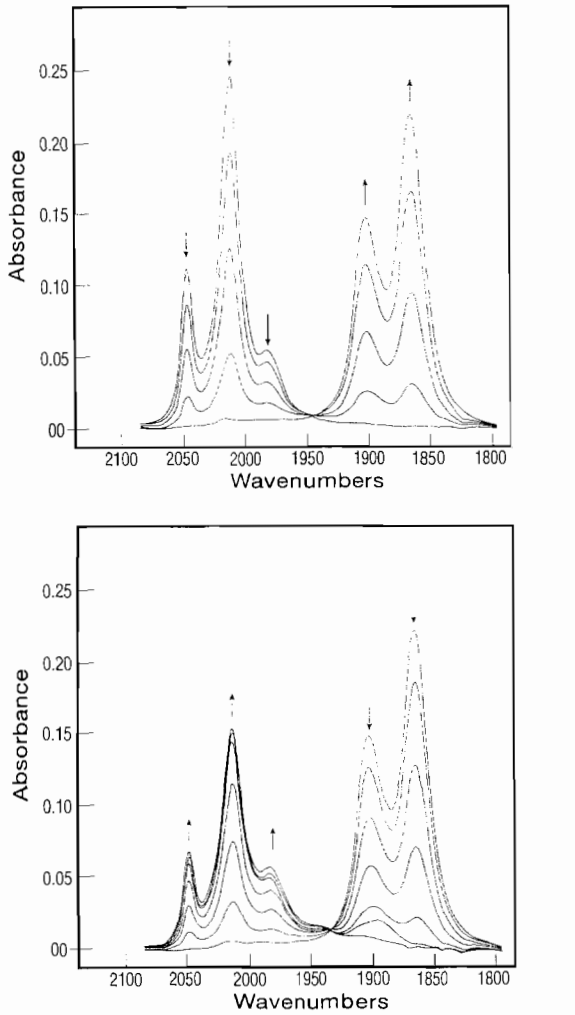

Fig. 8. (a) IR spectroelectrochemical reduction of $Mn_2(CO)_{10}$ in 0.1 M $TBA^+PF_6^-/CH_3CN$. (b) IR spectroelectrochemical oxidation of the product of (a).

(Fig. 8(b)) [3]. This latter result has been previously attributed to rapid coupling of the initially formed $Mn(CO)_5$ radical, which dimerizes near the diffusion-controlled limit [12]. Given that we observe no $Mn_2(CO)_{10}$ when $Mn(CO)_5^-$ is oxidized in the presence of $Rh_2(TM4)_4^{2+}$, we propose that the manganese anion and dirhodium dication form tight ion aggregates in CH_3CN, so that once generated, the $Mn(CO)_5$ radicals are completely scavenged by $Rh_2(TM4)_4^{2+}$ to form $Rh_2(TM4)_4(Mn(CO)_5)_2^{2+}$.

As previously reported, spectroelectrochemical oxidation of $Mn_2(CO)_{10}$ results in metal–metal bond cleavage, yielding the mononuclear species, $Mn(CO)_5(CH_3CN)^+$ (ν(CO) = 2160(vw), 2074 and 2056 cm^{-1}) [13]. Surprisingly, reduction of this cation occurs as a $2e^-$ process, yielding *not* $Mn_2(CO)_{10}$, but mononuclear $Mn(CO)_5^-$ (Fig. 9). In accord with the observations of Kochi and co-workers who investigated the electron-transfer kinetics of $Mn(CO)_5(CH_3CN)^+$ with $Mn(CO)_5^-$ [14], if the spectroelectrochemical reduction of $Mn(CO)_5(CH_3CN)^+$ is stopped midway through the process, the resulting 1:1 mixture of 'disproportionated' cation and anion is kinetically stable toward comproportionation over many minutes, despite the calculated driving force for the recombination reaction of ~10 kcal mol^{-1} [15]. This kinctic stability presumably originates from a slow initial electron transfer in which two $18e^-$ species are converted into $17e^-$ and $19e^-$ radical intermediates, respectively.

[3] As previously noted by Kadish and co-workers [11] the actual yield of $Mn_2(CO)_{10}$ formed during the electrochemical oxidation of $Mn(CO)_5^-$ depends on the applied potential: a potential significantly positive of the irreversible peak ($E_{pa} = -0.30$ V) results in a portion of the $Mn(CO)_5^-$ anion being directly oxidized to $Mn(CO)_5(CH_3CN)^+$.

4. Discussion

The metal–metal bond cleavage products that result from electrochemical oxidation and reduction of Rh_2-

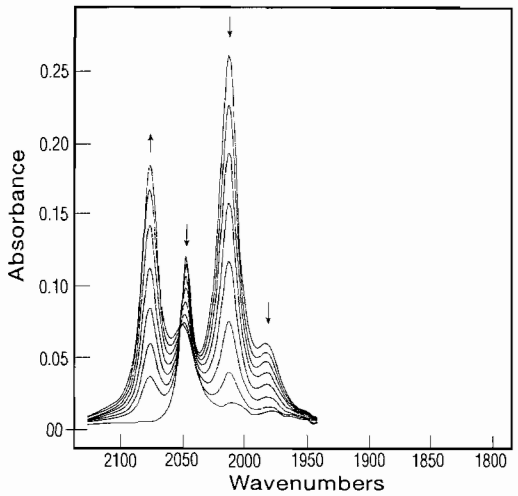

(a)

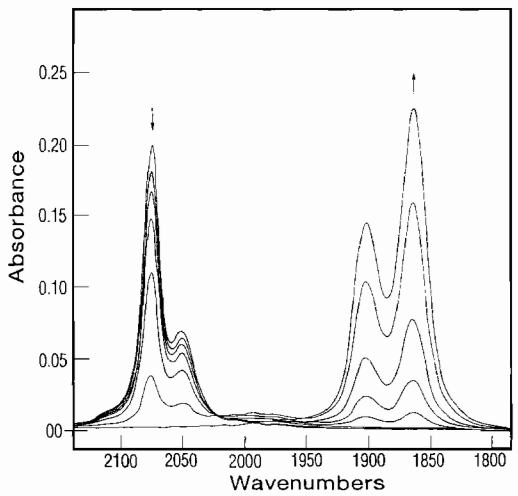

(b)

Fig. 9. (a) IR spectroelectrochemical oxidation of $Mn_2(CO)_{10}$ in 0.1 M $TBA^+PF_6^-/CH_3CN$. (b) IR spectroelectrochemical reduction of the resulting $Mn(CO)_5(CH_3CN)^+$ cation produced in (a). Product bands at 1901 and 1863 cm^{-1} are due to $Mn(CO)_5^-$.

$(TM4)_4(Mn(CO)_5)_2^{2+}$ and $Rh_2(TM4)_4(Re(CO)_5)_2^{2+}$ can be understood within the framework of a simple molecular orbital model developed previously [1b,3,4]. The metal–metal σ bonding can be described in a linear tetranuclear species with a Hückel-type molecular orbital scheme composed of levels derived from a metal d_{z^2} orbital on each center. The central (P(Rh–Rh)) and outer (P(M–Rh)) bond orders (neglecting overlaps) in terms of the mixing coefficients α and β have been calculated for relevant species containing 3 to 8 d_{z^2} electrons. Further, making the assumption of Miskowski and Gray [1b] that full delocalization is not energetically favorable [4], the maximum total bond order (P(total) = $2P$(M–Rh) + P(Rh–Rh)) is reached for all the various oxidation levels when $\alpha = \beta = (\sqrt{5}-1)/2 = 0.618$. Values for P(M–Rh), P(Rh–Rh) and P(total) are given in Table 2 for $\alpha = \beta = 0.618$.

Examination of the bond order values in Table 2 suggests that reduction of the $Rh_2(TM4)_4(M(CO)_5)_2^{2+}$ species ($6d_{z^2}$ electrons) by 2 electrons would result in the production of the neutral species, $Rh_2(TM4)_4(M(CO)_5)_2$. This species has a predicted bond order of 0 for both the M–Rh and Rh–Rh interactions and should be unstable with respect to loss of the $M(CO)_5^-$ units. Our spectroelectrochemical results show that the $2e^-$-reduction process produces $Rh_2(TM4)_4^{2+}$ and $M(CO)_5^-$, which interact only through ion-pairing. Reoxidation of the reduced solution efficiently reforms the $Rh_2(TM4)_4M(CO)_5)_2^{2+}$ species.

This simple bonding model also has some predictive value for the oxidation chemistry we have studied. As the $Rh_2(TM4)_4(M(CO)_5)_2^{2+}$ species is sequentially oxidized to $Rh_2(TM4)_4(M(CO)_5)_2^{3+}$ and then to $Rh_2(TM4)_4(M(CO)_5)_2^{4+}$, P(M–Rh) increases as P(Rh–Rh) decreases. (A decrease in P(Rh–Rh) does not cause disruption of the tetranuclear species because the Rh–Rh unit is bridged by the four diisocyanide units.) Thus the spectroscopic observation of the $Rh_2(TM4)_4(Re(CO)_5)_2^{3+}$ and $Rh_2(TM4)_4(Mn(CO)_5)_2^{4+}$ redox levels are consistent with the model. The apparent *instabilities* of $Rh_2(TM4)_4(Mn(CO)_5)_2^{3+}$ (with respect to disproportionation) and $Rh_2(TM4)_4(Re(CO)_5)_2^{4+}$ (with respect to Re–Rh bond cleavage) are *not* straightforwardly predicted by the model. Unanticipated steric

Table 2
Calculated bond orders[a] for relevant $Rh_2(TM4)_4(M(CO)_5)_2^{n+}$ species

n	No. of d_{z^2} e^-	P(M–Rh)[b]	P(Rh–Rh)[b]	P(total)[c]
5	3	0.67	0.59	1.93
4	4	0.89	0.45	2.24
3	5	0.67	0.59	1.93
2	6	0.45	0.72	1.62
1	7	0.22	0.36	0.81
0	8	0.00	0.00	0.00

[a]The four wavefunctions are:

$$\Psi_1 = \frac{(\alpha\phi_{M1} + \phi_{Rh1} + \phi_{Rh2} + \alpha\phi_{M2})}{\sqrt{(2+2\alpha^2)}};$$

$$\Psi_2 = \frac{(\phi_{M1} + \beta\phi_{Rh1} - \beta\phi_{Rh2} - \phi_{M2})}{\sqrt{(2+2\beta^2)}};$$

$$\Psi_3 = \frac{(\phi_{M1} - \alpha\phi_{Rh1} - \alpha\phi_{Rh2} + \phi_{M2})}{\sqrt{(2+2\alpha^2)}};$$

$$\Psi_4 = \frac{(-\beta\phi_{M1} + \phi_{Rh1} - \phi_{Rh2} + \beta\phi_{M2})}{\sqrt{(2+2\beta^2)}}.$$

[b]P(AB), bond orders, are calculated as $P(AB) = \Sigma_j n_j C_{Aj} C_{Bj}$ where the sum is taken over all occupied MOs; n_j is the number of electrons in the jth MO and C_{Aj} and C_{Bj} are the orbital coefficients of atoms A and B in the jth MO.

[c]P(total) = $2P$(M–Rh) + P(Rh–Rh).

[4] We believe that this assumption is not strictly applicable to the heteronuclear case discussed here, but the qualitative predictions it allows may still be valid.

effects or changes in the relative stabilities of mononuclear cleavage products (i.e. $Re(CO)_5(CH_3CN)^+$ versus $Mn(CO)_5(CH_3CN)^+$) may explain these deviations from the predictions. Again, in accord with experiment, the model correctly predicts that the oxidation of $Rh_2(TM4)_4(M(CO)_5)_2^{4+}$ to $Rh_2(TM4)_4(M(CO)_5)_2^{5+}$ should increase P(Rh–Rh) and decrease P(M–Rh). Experimentally, we observe that the oxidation of $Rh_2(TM4)_4(Mn(CO)_5)_2^{4+}$ leads to Mn–Rh bond cleavage to produce $Mn(CO)_5(CH_3CN)^+$ and $Rh_2(TM4)_4^{4+}$. As further developments of the synthetic chemistry and the model occur, a more detailed treatment of these redox reactions can be made.

Acknowledgements

We thank Dr Sam Kim at the Jet Propulsion Laboratory for the use of his EPR spectrometer. M.G.H. acknowledges the University of Minnesota graduate school for a Stanwood Johnston Memorial Fellowship. P.B. acknowledges the Lando-SOHIO foundation for an undergraduate research fellowship. This research was supported in part through a grant from the National Science Foundation.

References

[1] (a) K.R. Mann, M.J. DiPierro and T.P. Gill, *J. Am. Chem. Soc., 102* (1980) 3965; (b) V.M. Miskowski and H.B. Gray, *Inorg. Chem., 26* (1987) 1108.

[2] (a) B. Lippert, *Prog. Inorg. Chem., 37* (1989) 1; (b) T.V. O'Halloran, M.M. Roberts and S.J. Lippard, *J. Am. Chem. Soc., 106* (1984) 6427; (c) T.V. O'Halloran, P.K. Mascharak, I.D. Williams, M.M. Roberts and S.J. Lippard, *Inorg. Chem., 29* (1987) 1261.

[3] D.A. Bohling, T.P. Gill and K.R. Mann, *Inorg. Chem., 20* (1981) 194.

[4] M.M. Mixa, A.G. Sykes and K.R. Mann, *Inorg. Chim. Acta, 160* (1989) 159.

[5] H.M. Koepp, H. Wendt and H.Z. Strehlow, *Z. Elektrochem., 64* (1960) 483.

[6] R.R. Gagne, C.A. Koval and G.C. Kisensky, *Inorg. Chem., 19* (1980) 2854.

[7] J.P. Bullock and K.R. Mann, *Inorg. Chem., 28* (1989) 4006.

[8] S.P. Best, R.J.H. Clark, R.C.S. McQueen and R.P. Cooney, *Rev. Sci. Instrum., 58* (1987) 2071.

[9] (a) J.C. Hileman, D.K. Hueggins and H.D. Kaesz, *Inorg. Chem., 1* (1962) 933; (b) R. Ugo, S. Cenini and F. Bonati, *Inorg. Chim. Acta, 1* (1967) 451.

[10] M.G. Hill and K.R. Mann, *Catal. Lett., 11* (1991) 341.

[11] D.A. Lancombe, C.P. Anderson and K.M. Kadish, *Inorg. Chem., 25* (1986) 2074, and refs. therein.

[12] (a) M.S. Wrighton and D.S. Ginley, *J. Am. Chem. Soc., 97* (1975) 2065; (b) J.L. Hughey, C.P. Anderson and T.J. Meyer, *J. Organomet. Chem.*, (1977) C49; (c) W.L. Waltz, O. Hackelberg, L.M. Dorfman and A. Wojcicki, *J. Am. Chem. Soc., 100* (1978) 7259; (d) H.W. Walker, R.S. Herrick, R.J. Olsen and T.L. Brown, *Inorg. Chem., 23* (1984) 3748.

[13] J.P. Bullock, M.C. Palazzotto and K.R. Mann, *Inorg. Chem., 29* (1990) 4413.

[14] K.Y. Lee, D.J. Kuchynka and J.K. Kochi, *Organometallics, 6* (1987) 1886.

[15] J.R. Pugh and T.J. Meyer, *J. Am. Chem. Soc., 114* (1992) 3784.

[16] J.P. Bullock, *Ph.D. Thesis,* University of Minnesota, Minneapolis, MN, 1990.

[17] M.G. Hill, K.R. Mann, *Inorg. Chem., 32* (1993) 783.

[18] W. Tam, M. Marsi and J.A. Gladysz, *Inorg. Chem., 22* (1983) 1413.